UNIVERSITY OF LEEDS

This is a repository copy of *Adsorption and oxidation of NO and N2O on soot surfaces: Evolution of functional groups*.

White Rose Research Online URL for this paper:
https://eprints.whiterose.ac.uk/223623/

Version: Accepted Version

Article:
Jin, S., Fan, C., Fu, Z. et al. (6 more authors) (2025) Adsorption and oxidation of NO and N2O on soot surfaces: Evolution of functional groups. Fuel, 390. 134643. ISSN 0016-2361

https://doi.org/10.1016/j.fuel.2025.134643

Reuse
This article is distributed under the terms of the Creative Commons Attribution (CC BY) licence. This licence allows you to distribute, remix, tweak, and build upon the work, even commercially, as long as you credit the authors for the original work. More information and the full terms of the licence here: https://creativecommons.org/licenses/

Takedown
If you consider content in White Rose Research Online to be in breach of UK law, please notify us by emailing eprints@whiterose.ac.uk including the URL of the record and the reason for the withdrawal request.

White Rose university consortium
Universities of Leeds, Sheffield & York

eprints@whiterose.ac.uk
https://eprints.whiterose.ac.uk/

Adsorption and oxidation of NO and N_2O on soot surfaces: evolution of functional groups

Shuo Jin[a], Chenyang Fan[a*], Zheng Fu[a,b], Haizhao Li[a], Ye Liu[c*], Bin Xu[a], Huiyong Du[a], Guorong Lin[a], Mingliang Wei[b]

[a] *Henan Provincial International Joint Laboratory of Energy Conservation and Pollutant Control of Energy Power Equipment, College of Vehicle and Traffic Engineering, Henan University of Science and Technology, Luoyang 471003, China*

[b] *State Key Laboratory of Intelligent Agricultural Power Equipment, Luoyang 471003, China*

[c] *Institute for Transport Studies, University of Leeds, Leeds LS2 9JT, UK*

Corresponding author. Chenyang Fan and Ye Liu

E-mail address: fanchenyang@haust.edu.cn; Y.Liu8@leeds.ac.uk

Postal address: Vehicle & Transportation Engineering Institute, Henan University of Science and Technology, Luoyang 471003, China ; Institute for Transport Studies, University of Leeds, Leeds LS2 9JT, UK

Abstract

Co-firing ammonia with hydrocarbon fuel (such as methane) is an attractive method for reliable application of ammonia for power, and in this case the interaction of NO_x (NO, N_2O) and soot is possible. To reveal the interaction mechanism, the role of NO and N_2O in adsorption and oxidation processes on soot surfaces was investigated in terms of the evolutions of functional groups by thermogravimetric analysis (TGA), X-ray photoelectron spectroscopy (XPS) and Fourier transform infrared spectroscopy (FT-IR) technologies. During the adsorption and oxidation processes, the content of C-O groups on soot surfaces at NO and N_2O atmosphere is larger than that in air. C-O accumulated in the adsorption stage is prone to be converted into C=O and O=C-O in the oxidation stage. In addition, the N-O bonds on soot surfaces remained stable in air but underwent significant changes in the presence of NO_x. O atoms arise from air and N_2O may be more likely to replace the H atom on methyl or methylene on soot surfaces, while NO can not only attack C-H groups but also be prone to break C=C on aromatic rings. This study offers novel insights into the fuel-NO_x interactions with soot and is helpful for co-reducing soot and NO_x emissions from NH_3/hydrocarbon fuel combustion.

Keywords:

33 Soot, NO_x, Oxidation, Adsorption, Functional groups, Laminar diffusion flame

Nomenclature

TGA	thermogravimetric analysis
XPS	X-ray photoelectron spectroscopy
FT-IR	Fourier transform infrared spectroscopy
Re	Reynolds number
$A_{ali\text{-}C\text{–}H}/A_{C=C}$	the concentration of aliphatic C–H groups relative to the aromatic C=C
$A_{C=O}/A_{C=C}$	the concentration of C=O groups relative to the aromatic C=C
$A_{C\text{-}O}/A_{C=C}$	the concentration of C-O groups relative to the aromatic C=C
A_{ds} phase	Adsorption-dominated phase
O_{xi} phase	Oxidation-dominated phase.

1. Introduction

Energy is an integral material guarantee for the development of the national economy, and the exploration of energy determines the future development destiny of the country [1]. Nevertheless, the majority of the energy consumption structures is still reliant on fossil fuels such as coal and oil at the present moment [2], leading to the serious CO_2 emission of harmful pollutants that not only greatly impact human health but also aggravates the greenhouse effect. Intending to slash the carbon emissions, one of the key methods is to increase the usage of renewable, low-carbon or carbon-free fuels [3].

During the past few decades, ammonia (NH_3) has emerged as a potential alternative fuel owing to the high hydrogen density and carbon-free structure [4, 5]. Considering the higher ignition temperature and unstable combustion of pure ammonia fuel, it is difficult to directly apply pure ammonia fuel on internal combustion engines [6]. Therefore, in order to convert the fuel into ammonia step-by-step, it is considered to partially replace hydrocarbon with NH_3 [7]. At present, a large number of studies have shown that replacing part of hydrocarbon fuel with NH_3 will obviously reduce the carbon emissions [8-10]. However, co-firing of ammonia and hydrocarbon fuels may lead to new problems: NH_3 combustion could cause the most significant NO_x emissions

on account of fuel-bounded nitrogen [11-13], and insufficient combustion of hydrocarbon fuels leads to soot formation [14-16]. Moreover, different from the hydrocarbon fuels, the fuel-NO_x in ammonia flames is generated uniformly in the bulk combustion regions [17]. In this case, part of the fuel-NO_x generation region may overlap with the regions of soot formation and oxidation, yielding interaction of soot and NO_x. Possible interaction between NO_x and soot offers an alternative route to control their emissions at the same time. Consequently, it is of great significance to study the reaction mechanism between NO_x and soot.

Co-firing NH_3 with hydrocarbons will affect the emission of soot [7, 18]. As stated in Montgomery et al. [19], the concentration of soot in CH_4 combustion could be diminished by 10 times when ammonia doping was 20%. Bennett et al. [20] found that adding NH_3 into ethylene flames and reduce the soot concentration. Previous studies mainly focused on the soot and NO_x formation or emission of co-firing NH_3 with hydrocarbons [12, 20, 21], but the interaction between NO_x and soot was rarely studied without catalyst. Fortunately, there still are some studies that showed that NO_x could affect soot oxidation through chemical mechanisms. At a low temperature (250~400 °C), Müller et al. [22] found that NO_2 reduced the apparent activation of soot oxidation and promoted soot oxidation. According to Raj et al. [23], NO can eliminate

88 different types of reactive site present on soot and partial-oxidized soot. In addition,
89 Guo et al. [24] studied the effect of NO_x oxidation of soot under different catalysts.

90 Some studies have also found that NO_x can be absorbed on soot surfaces and
91 change the chemical bonds and functional groups. In a fixed-bed reactor, Klose et al.
92 [25] studied the adsorption of NO on activated carbon at 100 ℃, 120 ℃ and 150 ℃,
93 and found that there were four different NO adsorption species on activated carbon. As
94 stated in Abián et al. [26], they observed that the surface of soot formed nitrogen-
95 containing substances and some nitrogen seems to be combined with soot structure.
96 Specifically, Cao et al. [27] detected functional groups such as C-NO_2, C-ONO and C-
97 NCO on the surface of soot exposed in NO and O_2. The understanding of the functional
98 group on soot could shed more light on the impact of the chemical interaction of NO_x
99 with soot.

100 Compared to the amount of research carried out on NO, N_2O has been largely
101 disregarded, maybe for the reason that N_2O accounts for a small proportion in the NO_x
102 emissions [28]. However, N_2O is not only a greenhouse gas [29], but also its global
103 warming potential is 298 times that of CO_2 [30]. Carabineiro et al. [31] used N_2O to
104 oxidize commercial activated carbon under the condition of catalyst. The results of
105 temperature programmed experiments showed that the reaction products were CO_2 and

106 N_2. According to Zhu et al. [32], the reaction rate of N_2O with carbon is higher than that
107 of NO, but much lower than that of O_2. Most studies focus on the N_2O reaction with
108 carbon [28, 33], the reaction mechanism between N_2O and soot has not well been
109 understood.

110 However, due to the unclear reaction pathways of NO_x and soot, it remains
111 challenging to elucidate the suppressive effect of NO_x on soot. Therefore, this study
112 aims to understand the interaction mechanism of NO_x with soot particles in terms of
113 soot functional groups that reflects the routine and kinetics of surface reactions. The
114 evolution of functional groups on soot surfaces during adsorption and oxidation
115 processes of air, NO and N_2O were analyzed by TGA, XPS and FI-TR tests. The
116 findings of this work may benefit the understanding of the interaction of fuel-NO_x and
117 soot, and enable co-reduction of NO_x and soot emissions from ammonia/hydrocarbon
118 combustion.

119 2. Experimental

120 2.1 Sample preparation

121 In this study, particle samples were collected from a CH_4/air laminar coflow
122 diffusion flame on a Mckenna burner under controlled laboratory conditions. The
123 experimental schematic diagram of soot sampling is shown in Fig. 1. To ensure the

124 acquisition of sufficient material, the sampling duration was maintained for at least 30
125 minutes for each case. A quartz plate was positioned 50 mm above the burner. The flow
126 rate of CH_4 was set at 400 mL/min, while that of air was maintained at 15 l/min.
127 According to the method of [34], the Reynolds (Re) number under this experimental
128 condition is 62.2, ensuring that the flame belongs to a laminar diffusion flame. The soot
129 particles generated in the flame were deposited on the quartz glass. Then, the particles
130 were scraped from the plate and crushed into the powder. The sampling methods used
131 in the present work is based on the previous works by Yan et al. [35]. The soot particles
132 were then placed in a thermogravimetric analyzer (TGA2, Mettler-Toledo, Switzerland)
133 and were heated from the 30 ℃ to 900 ℃ to remove volatile compounds under N_2 gas
134 with the ramp rate of 25 ℃/min. After thermal treatment, each soot sample was heated
135 from 30 ℃ to the preset reaction temperature (200, 400, 600, 800 and 1000 ℃,
136 respectively) with the heating rate of 15 ℃/min in air (21% O_2 and 79% N_2), NO (1000
137 ppm) and N_2O (1000 ppm), respectively. After reaching the target temperature, the gas
138 flow was immediately switched to N_2 and cooled down to room temperature to obtain
139 soot samples. Finally, the resulting soot samples were sealed in drying cans for further
140 analysis. In the experiments, the gas flow rate was kept at 50 mL/min. In addition, the
141 pre-treated soot samples were mixed with KBr powder at a weight ratio of 0.5% and

142 then was fully mixed in a mortar to make a sample tablet for the FT-IR test.

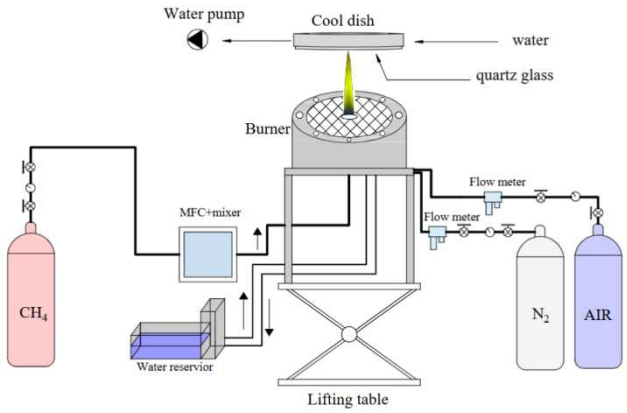

143

144 **Fig. 1.** Sampling device diagram.

145 2.2 Soot characterization

146 X-ray photoelectron spectroscopy (XPS) (Shimadzu/Kratos AXIS SUPRA^{+}) with

147 AlKa X-ray source was used to determine the oxygenated surface groups on the soot

148 surfaces. The C1s and O1s peaks were calibrated around 284.6 eV and 532.4 eV,

149 respectively. After extracting Sherley background with CasaXPS software package, the

150 C1s and O1s peaks were deconvolved to qualitatively and quantitatively represent the

151 binding state of carbon bonds and oxygenated surface groups, and the experimental

152 error was less than 5%.

153 A Fourier Transfer Inferred spectrometer (Bruker INVENIO-S) was employed to

154 assess the bulk chemistry of soot samples. The FT-IR ran under a spectral range of

155 400~4000 cm^{-1} with a resolution of 4 cm^{-1}. After the measurement under the set test

156 conditions, the baseline of FT-IR spectrum was corrected and smoothed by OMNIC

157 software (Thermo Nicolet). To ensure reproducibility, three FT-IR spectra are obtained
158 for each soot sample, and these FT-IR spectra are averaged to reduce noise. The
159 uncertainty of FT-IR results is less than 5%.

160 3. Results and discussion

161 *3.1 Oxidation behavior of soot samples*

162 In the present study, to eliminate the influence of sample mass variations, the soot
163 mass was normalized relative to the initial mass and presented as a percentage (%). Fig.
164 2 shows the normalized weight versus time curves of soot samples in the atmospheres
165 of air, NO and N_2O, respectively. In air atmosphere, no obvious mass loss was observed
166 in the range of 30~460 ℃, indicating that oxidation has not yet started. After 460 ℃,
167 the mass shows abruptly decrease in the mass until the temperature reaches 700 ℃.

168 Correspondingly, the initial oxidation temperature of soot in NO atmosphere is as
169 high as 700 ℃. The oxidation progresses in a distinct lower rate during the ramp up
170 profile from 700 to 1000 ℃. The soot burns out until the samples soaked for about 95
171 min at 1000 ℃. The onset and terminated temperatures are slightly higher than those
172 found by Xie et al. [36]. In the study of Xie, the lowest onset reaction temperature of
173 natural gas soot was 615~675 ℃ in the conditions of 200~1500 ppm NO. For N_2O
174 atmosphere, soot oxidation didn't start until 900 ℃. After annealing at 1000 ℃ for 317

175 min, the soot sample burns out.

176 Take the first derivative of the mass loss curve of soot in Fig. 2 to obtain Fig. 3.
177 Fig. 3 shows separately the oxidation rates curve of soot samples in the atmospheres of
178 air, NO and N_2O. The maximum oxidation rates of soot in air, NO and N_2O are 30, 1.4
179 and 0.65 %/min, respectively. Comparable results were also reported by Esarte et al.
180 [37] who compared the interaction of soot against O_2 and NO at 1000 °C. The results
181 showed that even if the initial concentration of oxygen (500 ppm) was lower than that
182 of NO (2000 ppm), soot samples are more active towards O_2 oxidation than towards
183 NO oxidation. Combined with Fig. (2-3), it can be found that N_2O not only has a low
184 oxidation rate, but also takes longer to oxidize soot with the same quality. Therefore,
185 the oxidation activity of soot in different atmospheres is air > NO > N_2O, respectively.

186 During the soot oxidation, the generation and transformation of functional groups
187 coinciding occurs on soot surfaces. Furthermore, their types and contributions are
188 mainly dependent upon the oxidation conditions [38, 39], and further reflecting the
189 oxidation degree [40, 41]. According to Azhagapillai et al. [42], they found that several
190 kinds of oxygenated functional groups (C = O, C-OH and C-O) were produced on the
191 surface of graphite after being oxidized by air. Besides ,Wang et al. [43] also found that
192 the concentration of aliphatic C-H, C-OH, and C-O groups on the surfaces of diesel

soots was related to the reaction atmosphere and soot oxidation degree. Moreover, the functional groups attached to soot surfaces show highly reactive edges, which provide reactive sites for the subsequent oxidation of soot particles [39, 43, 44]. Therefore, the scrutinization on the evolution of functional groups is also necessary to reveal the soot oxidation mechanism [39].

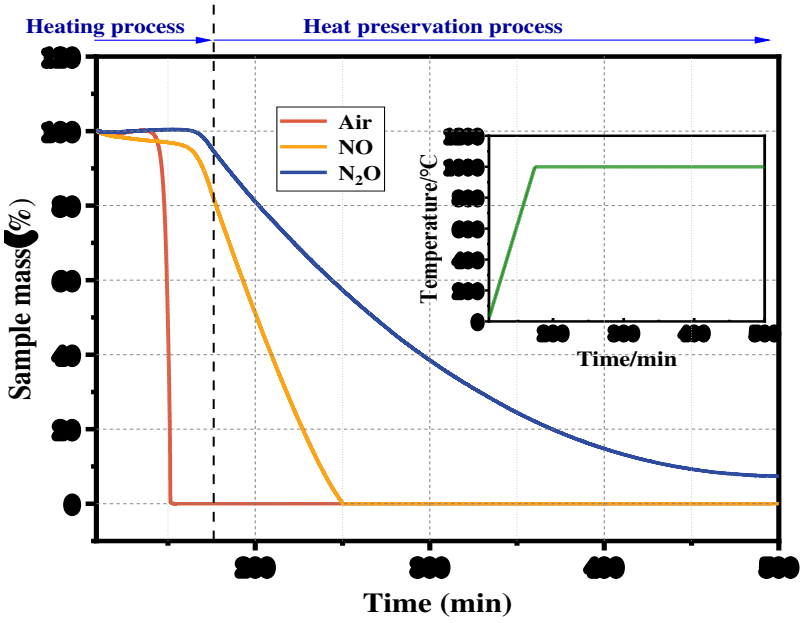

Fig. 2. The soot mass loss curves for TGA analysis.

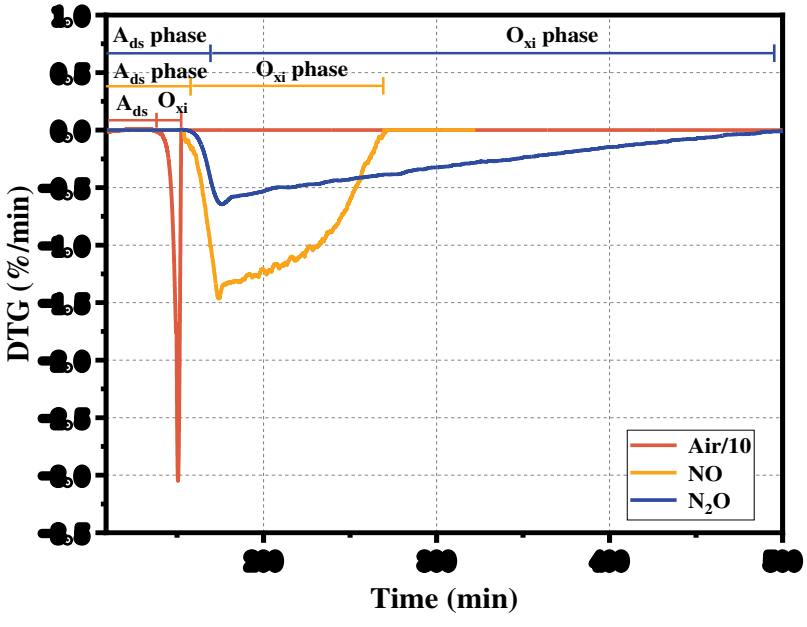

Fig. 3. DTG curves of the oxidation of the soot. A_{ds} phase- adsorption-dominated phase, O_{xi} phase-oxidation-dominated phase.

3.2 Oxygenated functional groups on soot surface

The X-ray photoelectron spectroscopy was used to determine the oxygenated surface groups and carbon bonding states on the soot surfaces in different oxidation atmospheres (Air, NO and N_2O).

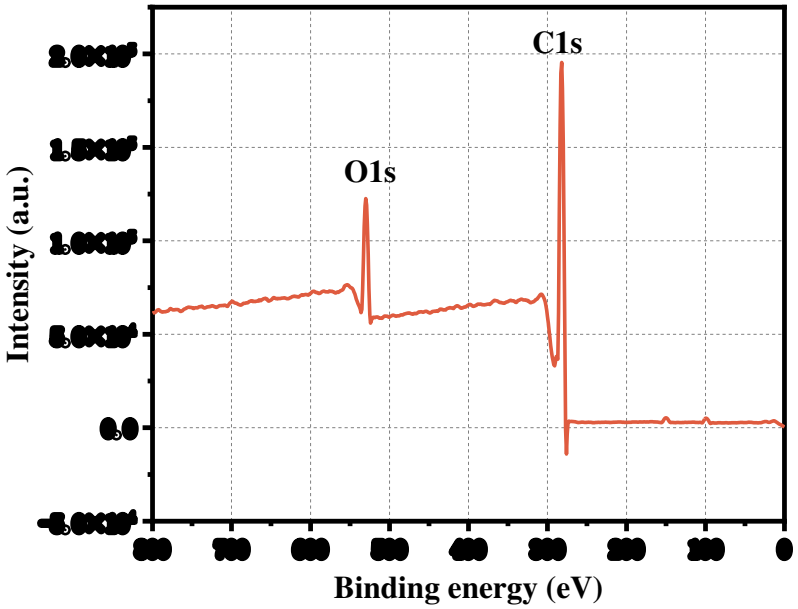

Fig. 4. Typical XPS survey scans of the original soot.

The XPS broad spectrum of original soot particles is shown in Fig. 4. It mainly consists of two peaks: O1s peak at ~533 eV and C1s peak at ~285 eV. The area ratio of these two peaks indicates the ratio of O and C atoms in soot particles [43, 44]. The O/C atomic ratio of soot particles is displayed in Fig. 5.

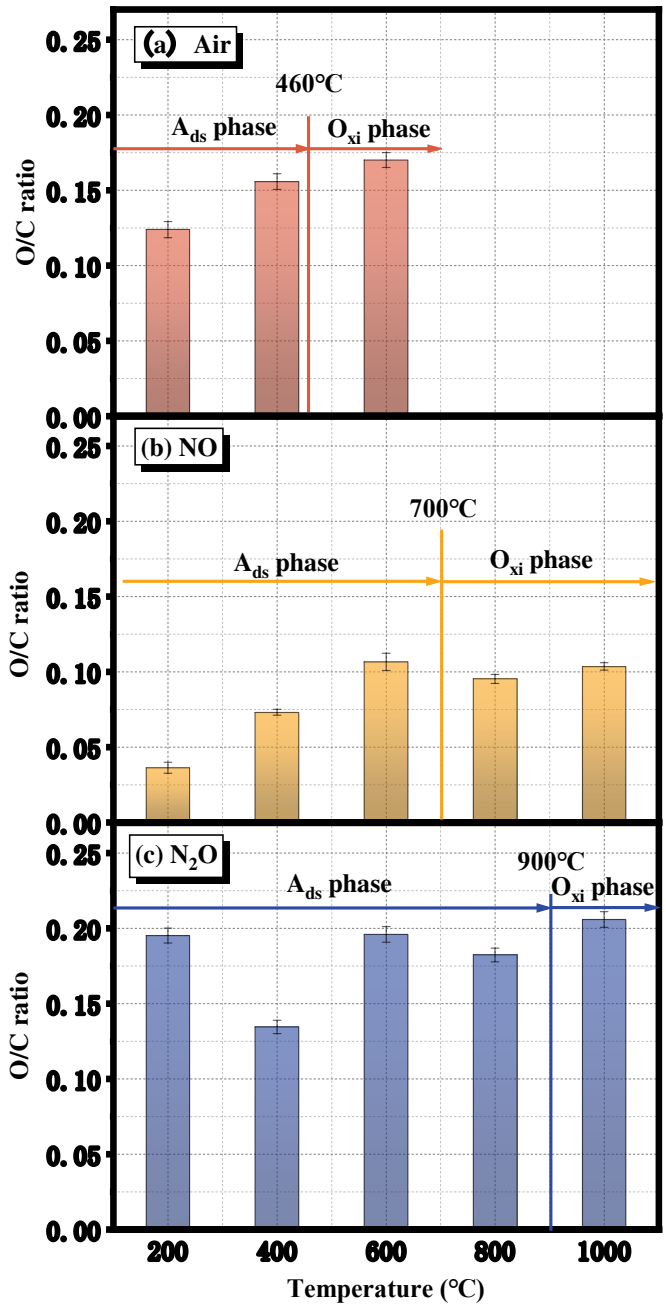

Fig. 5. O/C atomic ratios of soot particles at (a) Air, (b) NO and (c) N_2O atmospheres. A_{ds} phase- adsorption-dominated phase, O_{xi} phase- Oxidation-dominated phase. The error bars indicate the standard error.

Under the Air and NO atmospheres, the O/C atomic ratio of soot shows a consistent increase with the evolution of programmed oxidation from 200 to 600 °C. However, in N_2O atmosphere, the O/C atomic drops at 200~400 °C and rises at

400~600 ℃. For NO and N_2O, the O/C atomic ratio shows a decrease from 600 ℃ to 800 ℃ whereas reversely rises at 1000 ℃. The variation in O/C atomic ratios corresponds to the adsorption and oxidation processes. At the air atmosphere, the soot oxidation is not yet apparent under 200~460 ℃, while the O/C atomic ratio in Fig. 5 increased continuously, indicating that the adsorption on the soot surfaces is prevalence. Under 460~600 ℃, the drastic increase of O/C atomic ratio is coordinated with the sharp increase of oxidation rate. That is, the oxidation reactions may dominantly contribute to the rise of O/C ratio. The oxidation-induced increase of O/C atomic ratios was also found by Jeong et al. [45] who further concluded that the higher O/C ratio corresponded to a higher degree of oxidation. At the NO atmosphere, the mass loss of soot presents no obvious change at 200~700 ℃, and thus the increase in O/C atomic ratios here is mainly assigned to the adsorption of O atoms in NO on the active sites of soot surfaces [46]. When the temperature rises from 700 ℃ to 800 ℃, the O/C atomic ratio decreases in accordance with the moderate loss of soot mass. The O/C atomic ratio increases with the abruptly loss of soot mass from 800 ℃ to 1000 ℃. The increase of O/C ratio agrees well with the study of Leistner et al. [47]. During the reactions between diesel soot and NO at above 200 ℃, NO first adsorbed on the soot surface to form $C^*(NO)$ (the C^* may represent different types of activated carbon sites), and then

238 decomposed into $C^*(N)$ and $C^*(O)$, subsequently $C^*(N)$ was decomposed into N_2. As
239 stated by Suzuki et al. [48], NO reacts with soot above 600 ℃, consuming C*(O) to
240 produce CO_x. This may be the reason for the decrease of O/C ratio. Yang et al. [49]
241 found that the surface C(O) complex formed by NO adsorption on carbon black will
242 only decompose above 600℃. It is suggested that NO firstly reacts with carbon to form
243 C(O) and C(N) complexes. C(O) complexes decompose leading CO emission and
244 traces amount of CO_2. The statement may be a plausible factor for the reduction of O/C
245 ratio during the O_{xi} phase. At the N_2O atmosphere, during the heating process of
246 200~900 ℃, the change of O/C atomic ratio is solely attributed to the adsorption
247 processes, according to the insignificant mass loss of soot samples. The poor thermo-
248 dynamical stability of N_2O adsorption [50] may be responsible for the non-monotonic
249 evolution of O/C ratio at this A_{ds} phase. The oxidation process began to occupy a
250 dominant position at 900~1000 ℃, and the O/C atomic ratio increases rapidly at the
251 same time.

252 The higher the oxidation degree of soot, the more orderly the soot structure and
253 less sites available for the further adsorption and/or oxidation reactions. The sp^2 and sp^3
254 hybridized carbon atoms are integral to the overall soot nanostructure [39], and a large
255 sp^2/sp^3 hybridization ratio corresponds to a more ordered structure [51]. In the process

256 of soot oxidation, the existence of oxygenated functional groups provides quantities of
257 reactive sites for soot oxidation [39, 43, 44]. Moreover, surface functional groups are
258 most likely to associate with sp^2 and sp^3 carbon atoms located at the lamella edge and
259 interstitial sites [52]. Therefore, in order to better understand the adsorption and
260 oxidation mechanisms on soot surfaces, it is integral to gain insights into the sp^2/sp^3
261 hybridization ratio of C atoms and functional groups [43].

262 The sp^2/sp^3 hybridization ratio of C atom and the relative content of oxygenated
263 functional groups are derived from the high-resolution narrow spectrum of C1s after
264 deducting the background (Shirley). Due to the distinctly lower content of O than C
265 elements, it may be not very precise for the quantification of oxygenated functional
266 groups derived from C1s peaks. Fortunately, O1s peak can also provide important clues
267 about the evolution of oxygenated functional groups after oxidation [53]. Therefore, the
268 O1s peaks were also deconvolved to obtain the amount of these groups. The peak
269 assignments for C1s and O1s peaks are respectively listed in Tabs. 1 and 2, and the
270 fitting method is accordance with Fan et al. [53] and Simth et al. [54]. Typical C1s and
271 O1s spectra of the original soot are shown in Fig. 6.

272 **Tab. 1**

273 Band assignment of XPS narrow scan for soot particle samples from C1s

Peak	**BE(eV)**	**FWHM(eV)**	**References**
sp^2	284.3-284.8	1.2-2	[53, 55]

sp^3	285.0-285.6	1.2-2	[53, 55]
C-O groups in epoxy and/or C-OH /or C-N	286-286.6	1.2-2.2	[52, 55]
C=O groups in carbonyls	287-288.5	1.2-2.2	[55, 56]
O-C=O in carboxylic acid and ester groups	289-289.2	1.2-2.2	[55, 56]

Tab. 2

Band assignment of XPS narrow scan for soot particle samples from O1s.

Peak	**BE(eV)**	**FWHM(eV)**	**References**
C=O in quinone, carbonyl and/or carboxylic acid	530-532	1.2-2	[56, 57]
C-O in ether /C-OH	532.4-533.4	1.2-2.2	[56, 57]
COOH in carboxyl	533.4-534	1.2-2.2	[56, 57]
N-O	534-534.1	1.2-2.2	[56, 57]

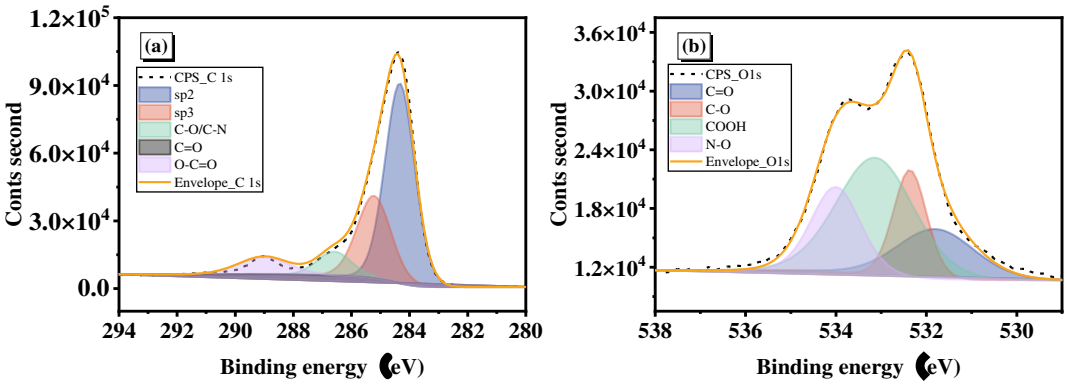

Fig. 6. Typical C1s (a) and O1s (b) spectra of the original soot.

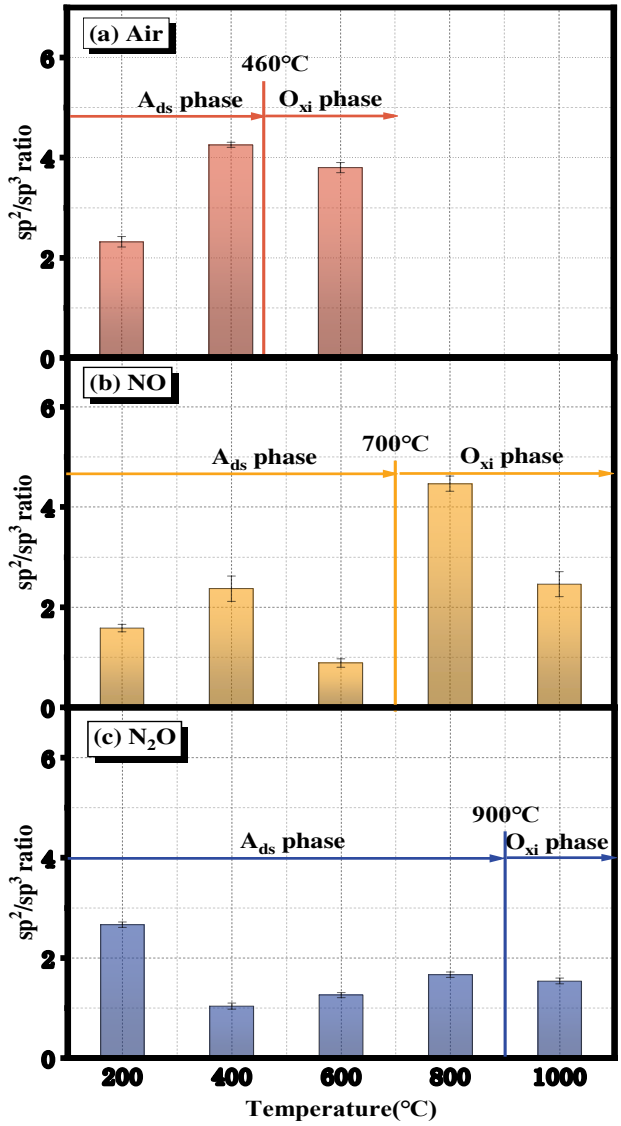

Fig. 7. Sp^2/sp^3 ratios of soot particles at (a) Air, (b) NO and (c) N_2O atmospheres. A_{ds} phase- adsorption-dominated phase, O_{xi} phase- Oxidation-dominated phase. The error bars indicate the standard error.

Sp^2 and sp^3 hybridization are the primary chemical state of carbon in soot, and the quantity and spatial relationship of carbon atoms in these two states are intimately associated with the oxidation of soot. Fig. 7 plots the sp^2/sp^3 hybridization ratios as functions of oxidation temperature. At the air, NO and N_2O atmosphere, soot particles

present significant difference in the evolution of sp^2/sp^3 ratio, with the increase, increase-then-decrease, and decrease-then-increase trends, respectively, during the A_{ds} phases. During the O_{xi} phase, the soot particles show consistently reduction in the sp^2/sp^3 ratio for the three atmospheres. The sp^2 hybridized carbons refer to ordered carbon in the lamellae, and the sp^3 hybridized carbons correspond to those at the defect sites that disturbs the sp^2 hybrid network [44, 51]. As a result, a higher sp^2/sp^3 hybridization ratio corresponds to the structure with less defects. A similar finding was reported by Gaddam et al. [58], who pointed out that the oxidation of the model carbon led to a slight decrease in the sp^2/sp^3 ratio from 460 ℃ to 600 ℃ .

Most of the O atoms are found within oxygenated functional groups that are chemically bonded to the soot surface, and their migration is related to the adsorption and oxidation on soot surfaces [59, 60].

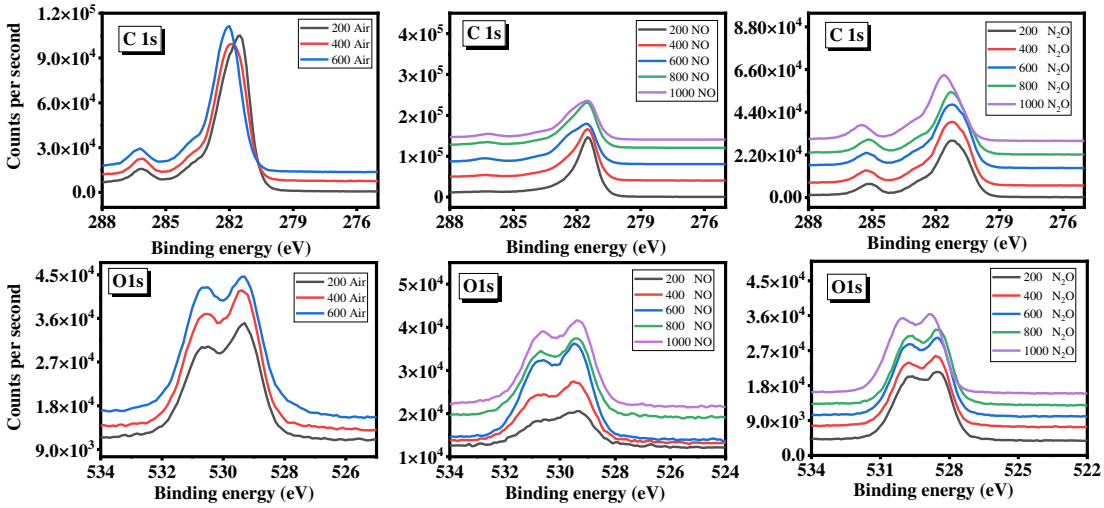

Fig. 8. The original spectral data of XPS measurements.

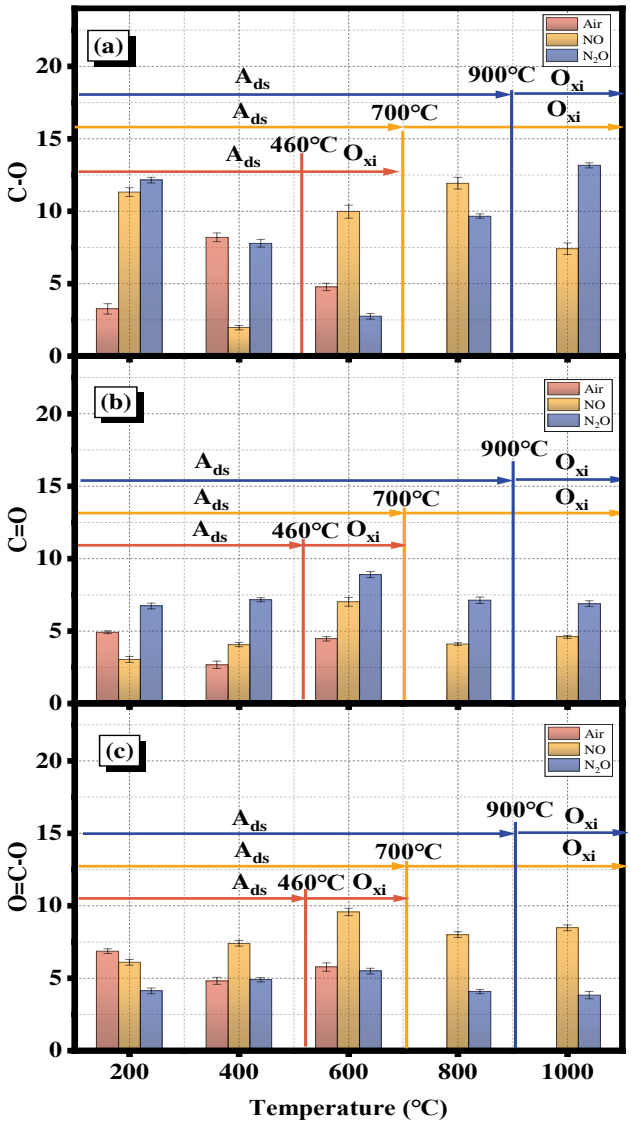

Fig. 9. Relative concentrations of oxygenated functional groups in C 1s for soot particles.

The error bars indicate the standard error.

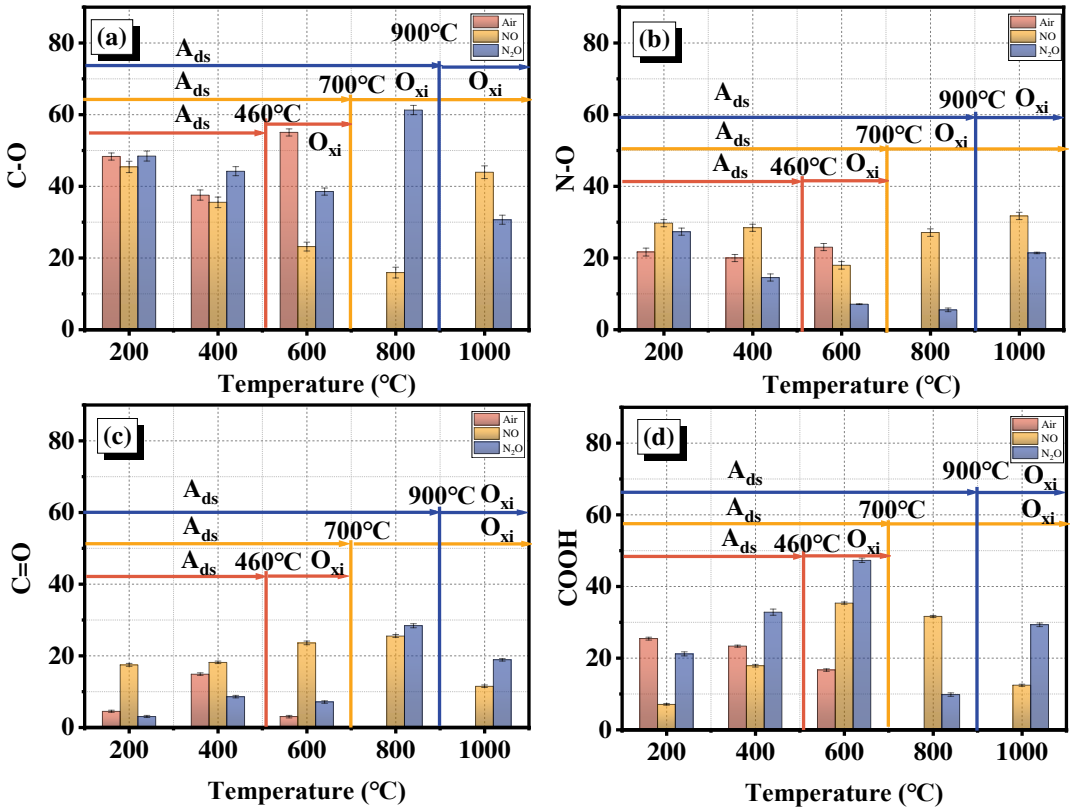

Fig. 10. Relative concentrations of oxygenated functional groups in O1s for soot particles. The error bars indicate the standard error.

Fig. 8 plots the original spectral data of XPS measurements. The content of oxygenated functional groups, as deconvolved from the C1s and O1s peaks, are illustrated in Figs. 9 and 10. The content of C-O groups in NO and N_2O is larger than that in air, meaning that C-O groups probably play a certain role in the reactions of NO_x with soot. This mechanism has been enhanced by Yan et al. [60], they found that the enrichment of C-O species could promote the oxidation of coal char. During the A_{ds} phases, the C-O (in epoxies) shows an increase for air atmosphere but consistent reduce-then-rise for the NO and N_2O atmospheres. Due to the adsorption of O on the surface of soot, a large amount of C(O) is produced [60], causing the accumulation of

C-O in the air atmosphere. The equation is gained for as follows [47, 61].

$$C^* + 1/2O_2 \rightarrow C^*(O) \quad (1)$$

$$C^* + NO \rightarrow C^*(N) + C^*(O) \quad (2)$$

$$C^* + N_2O \rightarrow N_2 + C(O) \quad (3)$$

The adsorption mechanism of NO on activated carbon had been studied by Wang et al. [62] , the C-O-NO was one of the products in the NO oxidation process[62]. The adsorption process of NO_x is also accompanied by the cracking and desorption of NO_x [63], O produced by NO_x cracking consumes C-O that may cause the decrease of C-O groups in the initial period of A_{ds} phase [47, 60, 61]. The enhancement of the NO_x adsorption gradually increases the C-O groups as the adsorption process evolves at the NO and N_2O atmospheres [47, 49, 64]. During the O_{xi} phases, the C-O (in epoxies) reduces for both air and NO conditions [47, 60], whereas increases under the N_2O atmosphere [61, 64]. The increase of temperature accelerates the change of oxygenated functional groups, and C-O is gradually consumed in the oxidation process, while C=O and O=C-O are gradually increased as oxidation products in the air atmosphere [65]. It is obvious that in these three atmospheres, the change of C=O (in carbonyls) and O=C-O (in carboxylic and esters) are synchronous, both of which are opposite to C-O groups as the A_{ds} and O_{xi} phase proceeds for all the three atmospheres. This inconsistence may

335 be responsible from the oxidation reactions, according to the conclusion drawn in [66],
336 epoxy groups are the dominant species at the low oxidation stage, and ethers and
337 carbonyls form as oxidation proceeds.

338 From O1s peaks, it is observed that at the air and NO conditions, the C-O bonds
339 (in ethers) on soot surfaces show consistent decrease during the A_{ds} phases for air and
340 NO conditions, whereas decrease-then-increase for the N_2O atmosphere. It is
341 noteworthy that the N-O varies in the same trends with the C-O bonds (in ethers) during
342 the A_{ds} phases. This finding also proves the generation of C-O-N=O resulting from the
343 NOx adsorption [62]. During the O_{xi} phases, the C-O species (in ethers) exhibit general
344 increase as the soot oxidation proceeds at the air and NO atmospheres but decrease at
345 the N_2O atmosphere. Wang et al. [62] found that NO adsorbed on the surface of carbon
346 materials would react with C=O and COOH to form C-O and N-O [62]. In addition, it
347 can be observed that N-O is relatively stable in air conditions, but it changes obviously
348 in NO and N_2O, suggesting that the N-O species may participate in the oxidation
349 reactions between soot and NO_x. Zhu et al. [50] studied the adsorption mode of NO and
350 N_2O, and found that they can react with the adsorption product C(N) and produce N_2
351 [49, 60, 61], but it was not observed that C(N) was consumed by O_2.

352 *3.3 Soot bulk chemistry*

As a surface analysis method, XPS provides the content and form of elements on the surface of the sample, rather than the overall composition of the sample [59]. It is quite different from that of the bulk phase, so there is often a difference between XPS and FT-IR, and the latter gives the information of bulk properties [67, 68]. In this study, the FT-IR spectra obtained at each case was normalized relative to the band intensity at~1620 cm^{-1} (aromatic C=C stretching vibration) to eliminate the influence of sample size on the band intensity [67, 69]. The peak assignments are demonstrated in Fig. 10. The FT-IR spectra of all soot particles possess similar contribution of peak positions, suggesting the similar functional group types within the soot samples [69]. Meanwhile, the samples show significant differences in peak intensity and profiles. Therefore, the FT-IR spectra were deconvoluted using Gaussian function for further quantity of the functional groups [67].

The most intensive absorption is detected at 3300~3650 cm^{-1}, corresponding to the stretching vibration of -OH groups [67, 69] that probably comes from carboxyls and phenols produced during soot oxidation [39, 43]. However, these peaks are easily interfered by the -OH within water molecules in lab atmosphere [39], so it is difficult to determine whether it arises from those bound by soot surfaces. Therefore, the peaks in this range are not analyzed in this paper. The peaks at 2975, 2925 and 2860 cm^{-1} are

assigned to aliphatic C-H functional groups [43, 44]. The band for C=O (coming from ketones, esters, anhydrides and lactones) is present near 1650~1860 cm^{-1} [39, 70]. The infrared absorption peak near ~1620cm^{-1} is the vibration peak of aromatic C=C [43, 44, 71]. The region between 1000 and 1300 cm^{-1} is a complex part of the spectra, where signals corresponding to aromatic C–C and C–H plane deformation structures may be overlapped with the signal corresponding to the stretching of C–O bands for carboxylic, anhydrides, esters and ether-like groups [39, 54, 70].

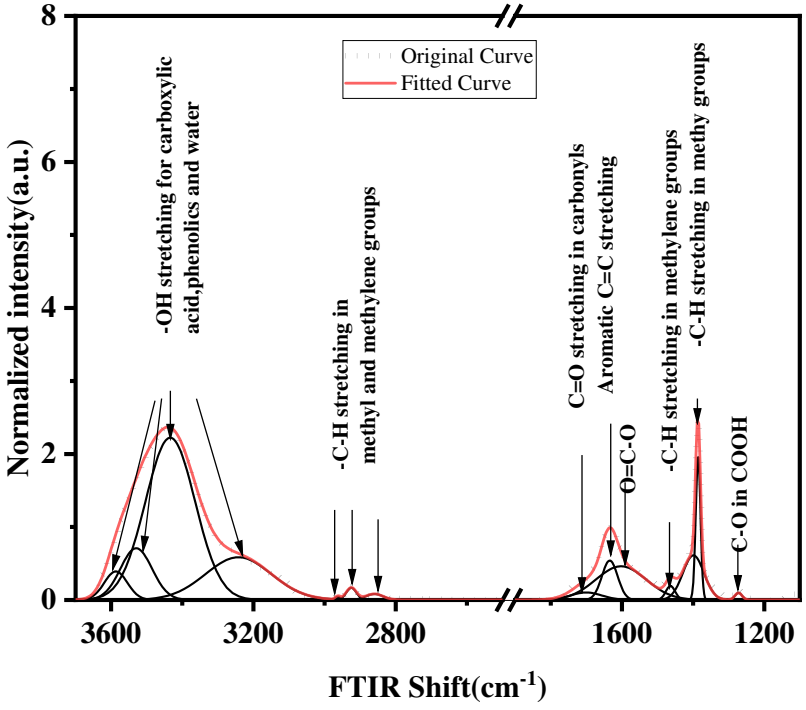

Fig. 11. Deconvolution of the typical FT-IR spectra and the peak assignment.

The peak area ratio (termed as $A_x/A_{C=C}$) of functional groups to aromatic group C=C can represent the concentration of functional groups [72]. Hereby, $A_{ali\text{-}C\text{–}H}/A_{C=C}$ represents the concentration of aliphatic C–H groups relative to the aromatic C=C

383 species. These aliphatic C-H functional groups are usually linked to the surface of
384 aromatic rings of PAHs in the form of aliphatic chain structures or saturated rings or
385 play a bridge role between different PAHs [73]. Nevertheless, aromatic C=C is on the
386 benzene ring, and the benzene ring is relatively stable, so it is tough to be substituted
387 and broken [71]. Hence, the dehydrogenation process of aliphatic C-H functional group
388 requires lower activation energy [43], which will increase the surface active sites of
389 soot particles and improve their oxidation activity [43, 53]. Evolutions of functional
390 groups are involved in their adsorption and oxidation reactions on soot surfaces [49].
391 That is, the adsorption, migration, desorption and oxidation at different positions on the
392 surface of soot [43, 74] may cause the transformation of aromatic C=C and aliphatic
393 C–H groups. Fig. 12 displays the variation in the ratio of $A_X/A_{C=C}$ of soot obtained under
394 different reaction conditions. At the air, NO and N_2O atmosphere, soot particles present
395 significant difference in the evolution of $A_{ali\ C–H}/A_{C=C}$ ratio, with the respectively
396 decrease, increase-then-decrease, and decrease trends, respectively, during the A_{ds}
397 phases. During the O_{xi} phases, the $A_{ali\ C–H}/A_{C=C}$ reduces for both air and N_2O conditions,
398 whereas increases under the NO atmosphere. Specifically, it can be observed that the
399 $A_{ali\ C–H}/A_{C=C}$ of air and N_2O is decreased in the whole adsorption and oxidation stage,
400 which may indicate that O in air and N_2O are more likely to replace H atoms on methyl

401 or methylene groups. Similar to the work of Zheng et al. [75], some functional groups,
402 such as -CH_3/-CH_2, were consumed during the reaction between coal samples and
403 oxygen molecules, which increased the concentration of functional groups such as C-
404 O and C-C. Additionally, Xin et al. [76] found that the ratio of C-H/C=C showed a
405 downward trend in the process of soot oxidation by air. This shows that during the
406 oxidation process, aliphatic C-H is constantly bound by oxidants to ensure
407 dehydrogenation and carbonization on the surface of soot. However, the $A_{ali\text{-}C\text{–}H}/A_{C=C}$
408 increased in NO atmosphere, which may be related to the breakage of C=C owing to
409 the active site on benzene ring replaced by NO. This phenomenon has also been
410 described in detail by Raj et al. [23], who found that the adsorption of NO would cause
411 the C=C fracture of benzene ring on soot using density functional theory and transition
412 state theory.

413 The content of C=O (in carbonyls) shows a decrease for air and N_2O atmosphere,
414 during the A_{ds} and O_{xi} phases. However, it shows rise-then-reduce during the A_{ds} phases
415 and rise during the O_{xi} phases under NO atmosphere. This evolution is inconsistent with
416 that for C=O in carbonyls obtained by XPS, which may mean that internal and surface
417 oxidation may exist simultaneously. During the A_{ds} phases for air, NO and N_2O
418 conditions, the content of C-O (in carboxylic) shows increase, decrease and increase-

then-decrease, respectively. On the counterpart, the content of C-O (in carboxylic) all shows increase during the O_{xi} phases. Although the variation of O=C-O groups (in carboxylic and esters) is also observed from the XPS results, the prevalent role of C-O (in carboxylic) in FT-IR results probably indicate that the contribution of C-O from carboxyl group is dominating rather than esters in the adsorption and oxidation processes of O_2, NO and N_2O.

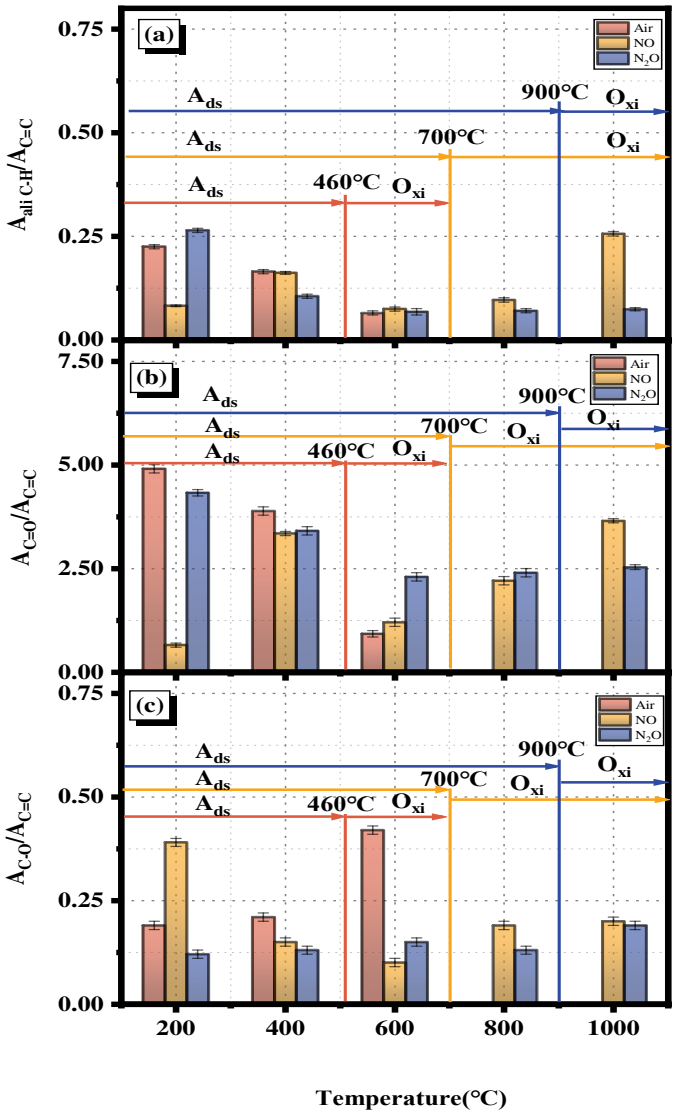

Fig. 12 Peak area ratio of aliphatic C-H, C=O and C-O groups to aromatic C=C group

derived from FT-IR spectrum of soot samples in air, NO and N_2O atmospheres. The error bars indicate the standard error.

4. Conclusion

To figure out the adsorption and oxidation mechanism of NO_x on soot, the surface chemical properties of soot before and after exposure to air, NO and N_2O were studied by TGA, XPS and FT-IR. The main findings are summarized as follows:

(1) The soot oxidation in air condition possesses highest activity, followed by NO and N_2O.

(2) During the adsorption and oxidation processes, the increase of C=O and O=C-O is accompanied by the decrease of C-O. Among them, the content of C-O groups in NO_x is higher. Meanwhile, the N-O decreases with the adsorption of NO and N_2O but increases during the oxidation phases. Conversely, the content of N-O groups keeps stable in air during both adsorption and oxidation processes.

(3) According to the different evolutions of aliphatic C-H/aromatic C=C, O atoms in air and N_2O may be more likely to replace H atom on methyl or methylene, while NO can not only attack C-H but also be prone to break C=C on benzene ring.

Investigating the interaction between NOx and soot not only enhances the understanding of NH_3/hydrocarbon co-combustion mechanisms but also offers a comprehensive theoretical foundation for the simultaneous control of soot and NOx

emissions from NH_3/hydrocarbon combustion systems. Future research should focus on exploring how this interaction influences the conversion processes of soot and NOx in aftertreatment devices, such as selective catalytic reduction (SCR) and diesel particulate filter (DPF) systems. Such studies are essential for effectively managing the final emissions from commercial NH_3/hydrocarbon-powered engines.

5. CRediT authorship contribution statement

Shuo Jin: Conceptualization, Investigation, Data visualization, Writing-original draft. **Chenyang Fan:** Investigation, Methodology, Funding acquisition, Project administration, Writing-review & editing. **Zheng Fu:** Investigation, Data visualization. **Bin Xu:** Investigation, Data visualization. **Guorong Lin:** Investigation, Data visualization, Validation. **Mingliang Wei**: Data Curation, Data visualization.

Acknowledgments

This research is sponsored by National Natural Science Foundation of China (No. 52006054), and International scientific and technological cooperation project in Henan Province (No. 232102521019)

References

[1] Ahmad T, Zhang D. A critical review of comparative global historical energy consumption and future demand: The story told so far. Energy Reports 2020;6:1973-91.

[2] Zou C, Zhao Q, Zhang G, Xiong B. Energy revolution: From a fossil

energy era to a new energy era. Natural Gas Industry B 2016;3(1):1-11.

[3] Han X, Wang Z, Costa M, Sun Z, He Y, Cen K. Experimental and kinetic modeling study of laminar burning velocities of NH_3/air, NH_3/H_2/air, NH_3/CO/air and NH_3/CH_4/air premixed flames. Combustion and Flame 2019;206:214-26.

[4] Xiao H, Lai S, Valera-Medina A, Li J, Liu J, Fu H. Study on counterflow premixed flames using high concentration ammonia mixed with methane. Fuel 2020;275:117902.

[5] Kobayashi H, Hayakawa A, Somarathne KKA, Okafor EC. Science and technology of ammonia combustion. Proceedings of the combustion institute 2019;37(1):109-33.

[6] Ichikawa A, Naito Y, Hayakawa A, Kudo T, Kobayashi H. Burning velocity and flame structure of CH_4/NH_3/air turbulent premixed flames at high pressure. International Journal of Hydrogen Energy 2019;44(13):6991-9.

[7] Yang Y, Zheng S, Wang H, Hu B, Liu H, Sui R, et al. Enhanced C_2-CN sub-mechanism: Impact on NO/N_2O and soot precursor yields during C_2H_2/HCN oxidation. Combustion and Flame 2024;260:113267.

[8] Lee H, Lee M-J. Recent advances in ammonia combustion technology in thermal power generation system for carbon emission reduction. Energies 2021;14(18):5604.

[9] Wang G, Guiberti TF, Cardona S, Jimenez CA, Roberts WL. Effects of residence time on the NO_x emissions of premixed ammonia-methane-air swirling flames at elevated pressure. Proceedings of the Combustion Institute 2023;39(4):4277-88.

[10] Ku JW, Choi S, Kim HK, Lee S, Kwon OC. Extinction limits and structure of counterflow nonpremixed methane-ammonia/air flames. Energy 2018;165:314-25.

[11] Okafor EC, Naito Y, Colson S, Ichikawa A, Kudo T, Hayakawa A, et al. Experimental and numerical study of the laminar burning velocity of CH_4–NH_3–air premixed flames. Combustion and flame 2018;187:185-98.

[12] Ariemma GB, Sorrentino G, Ragucci R, de Joannon M, Sabia P. Ammonia/Methane combustion: stability and NO_x emissions.

Combustion and Flame 2022;241:112071.
[13] Yang Y, Zheng S, Sui R, Lu Q. Impact of ammonia addition on soot and NO/N_2O formation in methane/air co-flow diffusion flames. Combustion and Flame 2023;247:112483.
[14] Chu H, Han W, Cao W, Gu M, Xu G. Effect of methane addition to ethylene on the morphology and size distribution of soot in a laminar co-flow diffusion flame. Energy 2019;166:392-400.
[15] Martin JW, Salamanca M, Kraft M. Soot inception: Carbonaceous nanoparticle formation in flames. Progress in Energy and Combustion Science 2022;88:100956.
[16] Dong W, Hong R, Yang Y, Wang D, Qiu B, Chu H. Analysis of the nanostructure evolution of soot in n-heptane/iso-octane with 2, 5-dimethylfuran addition: A combined experimental study and ReaxFF MD simulations. Combustion and Flame 2024;270:113751.
[17] Duynslaegher C, Contino F, Vandooren J, Jeanmart H. Modeling of ammonia combustion at low pressure. Combustion and Flame 2012;159(9):2799-805.
[18] Liu Y, Cheng X, Li Y, Qiu L, Wang X, Xu Y. Effects of ammonia addition on soot formation in ethylene laminar diffusion flames. Fuel 2021;292:120416.
[19] Montgomery MJ, Kwon H, Dreyer JA, Xuan Y, McEnally CS, Pfefferle LD. Effect of ammonia addition on suppressing soot formation in methane co-flow diffusion flames. Proceedings of the Combustion Institute 2021;38(2):2497-505.
[20] Bennett AM, Liu P, Li Z, Kharbatia NM, Boyette W, Masri AR, et al. Soot formation in laminar flames of ethylene/ammonia. Combustion and flame 2020;220:210-8.
[21] Cheng X, Li Y, Xu Y, Liu Y, Wang B. Study of effects of ammonia addition on soot formation characteristics in n-heptane co-flow laminar diffusion flames. Combustion and Flame 2022;235:111683.
[22] Müller J-O, Frank B, Jentoft RE, Schlögl R, Su DS. The oxidation of soot particulate in the presence of NO2. Catalysis today 2012;191(1):106-11.
[23] Raj A, Zainuddin Z, Sander M, Kraft M. A mechanistic study on the simultaneous elimination of soot and nitric oxide from engine exhaust. Carbon 2011;49(5):1516-31.

[24] Guo Q, Liu Y, Zhang X, Xu Y, Liu P, Zhang C. Enhanced NO_x-assisted soot combustion by cobalt doping to weaken mullite Mn-O bonds for lattice oxygen activation. Journal of Hazardous Materials 2025;482:136474.
[25] Klose W, Rincón S. Adsorption and reaction of NO on activated carbon in the presence of oxygen and water vapour. Fuel 2007;86(1-2):203-9.
[26] Abián M, Peribáñez E, Millera Á, Bilbao R, Alzueta MU. Impact of nitrogen oxides (NO, NO_2, N_2O) on the formation of soot. Combustion and flame 2014;161(1):280-7.
[27] Cao F, Chen J, Ni M, Song H, Xiao G, Wu W, et al. Adsorption of NO on ordered mesoporous carbon and its improvement by cerium. RSC Advances 2014;4(31):16281-9.
[28] Carabineiro SA, Lobo LS. Understanding the reactions of CO_2, NO, and N_2O with activated carbon catalyzed by binary mixtures. Energy & Fuels 2016;30(9):6881-91.
[29] Gao Z, Yang W, Ding X, Ding Y, Yan W. Theoretical research on heterogeneous reduction of N_2O by char. Applied Thermal Engineering 2017;126:28-36.
[30] Feng X, Gao H, Lal R, Zhu P, Peng C, Deng A, et al. Nitrous oxide emission, global warming potential, and denitrifier abundances as affected by long-term fertilization on Mollisols of Northeastern China. Archives of Agronomy and Soil Science 2019;65(13):1831-44.
[31] AC CSn, Sousa LL. Understanding the Reactions of CO_2, NO, and N_2O with Activated Carbon Catalyzed by Binary Mixtures. 2016.
[32] Zhu Z, Lu G. New insights into NO− carbon and N_2O− carbon reactions from quantum mechanical calculations. Energy & fuels 2003;17(4):1057-61.
[33] Hu X, Wang Y, Wu R, Zhao Y. Graphitic carbon nitride-supported cobalt oxides as a potential catalyst for decomposition of N2O. Applied Surface Science 2021;538:148157.
[34] White FM, Xue H. Fluid mechanics. McGraw-hill New York; 2003.
[35] Yan Z, Zhu T, Xue X, Liu H, Li Q, Huang Z. Effects of NH_3 and H_2 addition on morphology, nanostructure and oxidation of soot in n-decane diffusion flames. Fuel Processing Technology

2024;253:108003.
[36] Xie G, Fan W, Song Z, Lu J, Yu J, Zhang M. Experimental study on soot combustion and its noncatalyzed reaction with NO. Energy & fuels 2007;21(6):3134-43.
[37] Esarte C, Callejas A, Millera Á, Bilbao R, Alzueta MU. Characterization and reactivity with NO/O_2 of the soot formed in the pyrolysis of acetylene–ethanol mixtures. Journal of Analytical and Applied Pyrolysis 2012;94:68-74.
[38] Wei J, Lu W, Zeng Y, Huang H, Pan M, Liu Y. Physicochemical properties and oxidation reactivity of exhaust soot from a modern diesel engine: Effect of oxyfuel type. Combustion and Flame 2022;238:111940.
[39] Liu Y, Wu S, Fan C, Wang X, Liu F, Chen H. Variations in surface functional groups, carbon chemical state and graphitization degree during thermal deactivation of diesel soot particles. Journal of Environmental Sciences 2023;124:678-87.
[40] Schuster ME. Structure and Reactivity of Diesel Soot Particles from Advanced Motor Technologies. Technische Universität Berlin; 2010.
[41] Dong W, Hong R, Feng S, Qiu B, Fang R, Chu H. Synergistic effects of ether oxygen bond/benzene rin and hydrocarbon chain structure on soot morphology and nanostructure. Fuel 2025;381:133362.
[42] Azhagapillai P, Raj A, Elkadi M, Ali M. Role of oxygenated surface functional groups on the reactivity of soot particles: an experimental study. Combustion and Flame 2022;246:112436.
[43] Wang L, Song C, Song J, Lv G, Pang H, Zhang W. Aliphatic C–H and oxygenated surface functional groups of diesel in-cylinder soot: Characterizations and impact on soot oxidation behavior. Proceedings of the Combustion Institute 2013;34(2):3099-106.
[44] Liu Y, Song C, Lv G, Cao X, Wang L, Qiao Y, et al. Surface functional groups and sp3/sp2 hybridization ratios of in-cylinder soot from a diesel engine fueled with n-heptane and n-heptane/toluene. Fuel 2016;179:108-13.
[45] Jeong H, Jin M, So K, Lim S, Lee Y. Tailoring the characteristics of graphite oxides by different oxidation times. Journal of Physics D: Applied Physics 2009;42(6):065418.
[46] Sander M, Raj A, Inderwildi O, Kraft M, Kureti S, Bockhorn H. The

610 simultaneous reduction of nitric oxide and soot in emissions from
611 diesel engines. Carbon 2009;47(3):866-75.
612 [47] Leistner K, Nicolle A, Da Costa P. Detailed kinetic analysis of soot
613 oxidation by NO_2, NO, and NO+ O_2. The Journal of Physical
614 Chemistry C 2012;116(7):4642-54.
615 [48] Suzuki T, Kyotani T, Tomita A. Study on the carbon-nitric oxide
616 reaction in the presence of oxygen. Industrial & engineering
617 chemistry research 1994;33(11):2840-5.
618 [49] Yang J, Mestl G, Herein D, Schlögl R, Find J. Reaction of NO with
619 carbonaceous materials: 1. Reaction and adsorption of NO on
620 ashless carbon black. Carbon 2000;38(5):715-27.
621 [50] Zhu Z, Finnerty J, Lu G, Yang R. Opposite roles of O_2 in NO− and
622 N_2O− carbon reactions: an ab initio study. The Journal of Physical
623 Chemistry B 2001;105(4):821-30.
624 [51] Alfè M, Apicella B, Barbella R, Rouzaud J-N, Tregrossi A, Ciajolo
625 A. Structure–property relationship in nanostructures of young and
626 mature soot in premixed flames. Proceedings of the Combustion
627 Institute 2009;32(1):697-704.
628 [52] Vander Wal RL, Bryg VM, Hays MD. Fingerprinting soot (towards
629 source identification): Physical structure and chemical composition.
630 Journal of Aerosol Science 2010;41(1):108-17.
631 [53] Fan C, Wei J, Huang H, Pan M, Fu Z. Chemical feature of the soot
632 emissions from a diesel engine fueled with methanol-diesel blends.
633 Fuel 2021;297:120739.
634 [54] Smith M, Scudiero L, Espinal J, McEwen J-S, Garcia-Perez M.
635 Improving the deconvolution and interpretation of XPS spectra from
636 chars by ab initio calculations. Carbon 2016;110:155-71.
637 [55] Gaddam CK, Vander Wal RL. Physical and chemical
638 characterization of SIDI engine particulates. Combustion and Flame
639 2013;160(11):2517-28.
640 [56] Seong HJ, Boehman AL. Studies of soot oxidative reactivity using a
641 diffusion flame burner. Combustion and flame 2012;159(5):1864-75.
642 [57] Seong HJ, Boehman AL. Impact of intake oxygen enrichment on
643 oxidative reactivity and properties of diesel soot. Energy & fuels
644 2011;25(2):602-16.
645 [58] Gaddam CK, Vander Wal RL, Chen X, Yezerets A, Kamasamudram

K. Reconciliation of carbon oxidation rates and activation energies based on changing nanostructure. Carbon 2016;98:545-56.
[59] Vander Wal RL, Bryg VM, Hays MD. XPS analysis of combustion aerosols for chemical composition, surface chemistry, and carbon chemical state. Analytical chemistry 2011;83(6):1924-30.
[60] Yan W, Li S, Fan C, Deng S. Effect of surface carbon-oxygen complexes during NO reduction by coal char. Fuel 2017;204:40-6.
[61] Stanmore B, Tschamber V, Brilhac J-F. Oxidation of carbon by NO_x, with particular reference to NO_2 and N_2O. Fuel 2008;87(2):131-46.
[62] Wang D, Yang J, Ma S, Huo X. Efficient adsorption of NO onto K, Na-embedded porous carbon material prepared by using zinc-bearing dust as activator. Separation and Purification Technology 2024;348:127713.
[63] Li Z, Zhang W, Chen Z, Zhang Q, Yang X, Mao S, et al. Reaction mechanism for NO oxidation on the soot surface using a quantum chemistry. Fuel 2022;313:123032.
[64] Chen P, Gu M, Liu F, Chen J, Wang J, Lin Y. The effect of oxygen played in nitrous oxide heterogeneous reduction and the behavior of oxygen on char surface: quantum chemical and kinetics calculations. Combustion Science and Technology 2020;192(9):1682-706.
[65] Ma X, Song C, Wang X. Effects of temperatureon surface functional groups and oxidation reactivity of soot inmethane/oxygen premixed flames. Journal of CombustionScience and Technology 2014;20(2):170-5.
[66] Larciprete R, Lacovig P, Gardonio S, Baraldi A, Lizzit S. Atomic oxygen on graphite: chemical characterization and thermal reduction. The Journal of Physical Chemistry C 2012;116(18):9900-8.
[67] Winiarski J, Tylus W, Winiarska K, Szczygieł I, Szczygieł B. XPS and FT‐IR Characterization of Selected Synthetic Corrosion Products of Zinc Expected in Neutral Environment Containing Chloride Ions. Journal of Spectroscopy 2018;2018(1):2079278.
[68] Morozov IG, Belousova O, Ortega D, Mafina M-K, Kuznetcov M. Structural, optical, XPS and magnetic properties of Zn particles capped by ZnO nanoparticles. Journal of Alloys and Compounds 2015;633:237-45.
[69] Asemani M, Rabbani AR. Detailed FTIR spectroscopy

characterization of crude oil extracted asphaltenes: Curve resolve of overlapping bands. Journal of Petroleum Science and Engineering 2020;185:106618.
[70] Fan C, Guan Z, Wei J, Pan M, Huang H, Wei M. An assessment of soot chemical property from a modern diesel engine fueled with dimethyl carbonate-diesel blends. Fuel 2022;309:122220.
[71] Zygogianni A, Syrigou M, Konstandopoulos AG, Kostoglou M. Oxidative reactivity of particulate samples from different diesel combustion systems and its relation to structural and spectral characteristics of soot. Emission Control Science and Technology 2019;5:99-123.
[72] Russo C, Stanzione F, Tregrossi A, Ciajolo A. Infrared spectroscopy of some carbon-based materials relevant in combustion: qualitative and quantitative analysis of hydrogen. Carbon 2014;74:127-38.
[73] Peña GDG, Alrefaai MM, Yang SY, Raj A, Brito JL, Stephen S, et al. Effects of methyl group on aromatic hydrocarbons on the nanostructures and oxidative reactivity of combustion-generated soot. Combustion and Flame 2016;172:1-12.
[74] Gao Z, Zhu L, Liu C, Li A, He Z, Zhang C, et al. Comparison of soot formation, evolution, and oxidation reactivity of two biodiesel surrogates. Energy & Fuels 2017;31(8):8655-64.
[75] Zheng Y, Li Q, Lin B, Zhou Y, Liu Q, Zhang G, et al. Real-time analysis of the changing trends of functional groups and corresponding gas generated law during coal spontaneous combustion. Fuel Processing Technology 2020;199:106237.
[76] Wang X, Wei J, Zeng Y, Qian Y. Diesel soot combustion in air-NO environment: Evolution of functional groups on soot surfaces. Science of the Total Environment 2024;918:170579.